

Relaxed Nonlinear Vector Fitting for Calculation of Rational Approximation of Systems Defined by Input/Output Responses in the Frequency Domain

Abner Ramirez¹, Senior Member, IEEE, and Bjørn Gustavsen², Fellow, IEEE

Abstract—The so-called non-linear vector fitting (NL-VF) technique was recently introduced as a new method for rational function approximation in the frequency domain (FD). While the classical vector fitting (VF) fits a rational function to a given frequency response, NL-VF calculates the rational function approximation based on a set of input/output responses that characterize the system. The frequency responses can come from time domain (TD) responses that are transformed to the FD using the Numerical Laplace Transform (NLT), or it can be the set of frequency responses that result when characterizing non-linear systems in the FD, at a given operating point. This paper extends NL-VF to its relaxed version by replacing the scaling function used for pole relocation by a more relaxed constraint, following a similar approach as in the relaxed VF method. This paper shows that the relaxed NL-VF exhibits an improvement in both convergence and accuracy, as compared to its original formulation. The advantages are demonstrated for three examples of rational function approximation, 1) FD transfer function of a transmission line propagation function, 2) FD input/output variables of a system which includes a photovoltaic generator and a nonlinear reactor, and 3) TD measurements of an automatic voltage regulator response.

Index Terms—Rational fitting, system identification, electromagnetic transient analysis.

I. INTRODUCTION

RATIONAL function identification of dynamic systems has recently received a great deal of attention due to its wide range of applications in electrical power systems and other engineering areas [1]. Generally, rational function identification techniques are restricted to systems and devices that are linear in their input/output behavior, although in the real world, nonlinearities are intrinsic of dynamic systems.

Classical VF is tailored for linear systems. It provides a rational function approximation of a given frequency domain response, without relying on input/output variables [1]. The solving process relocates a set of initial poles to better positions

by repeated solving of an overdetermined linear least squares problem.

There exist methods that identify a dynamic system as a rational function by utilizing time-domain (TD) input/output variables, e.g., time domain VF (TD-VF) [2], [3], [4]. This type of identification allows to account for non-linear component effects, around an operating point, in the *black-box* part of the system. The recently introduced NL-VF approach, which uses frequency domain input/output variables, has shown some advantages over TD-based methods regarding computational efficiency and accuracy, e.g., NL-VF avoids TD convolution, as opposed to TD-VF [5]. It is mentioned that the word *non-linear* in the name “NL-VF” refers to the system to be identified and not to the method itself.

Both TD-VF and NL-VF can identify a system whose input/output signals come from the linearized version of the non-linear dynamic system at a specific operating point, or from the non-linear system for a specific set of parameters. Moreover, both can identify an intrinsically non-linear system based on measurements at the black-box terminals. A different identification has to be carried out for each distinct operating point, resulting in a new model.

TD-VF is restricted to TD input/output responses, either obtained from measurements or from analytical calculations. Those TD signals can also be obtained from their frequency domain counterparts, for instance by using the inverse NLT [6]. On the other hand, NL-VF handles frequency domain input/output signals obtained from measurements or, alternatively, from a TD simulation followed by NLT [6]. Nonetheless, as mentioned before, NL-VF presents advantages over TD-VF.

In the classical VF, [7], a rational scaling function $\sigma(s)$ is responsible for the pole relocation process, where $\sigma(s)$ approaches unity at infinite frequency to avoid the trivial (null) solution. The use of an asymptotic constraint negatively affects the pole relocation properties by reducing convergence speed and impairing the final result. This difficulty was overcome in [8] by introducing a new scaling function which does not include an asymptotic constraint. The resulting (relaxed) VF method was shown to have improved convergence properties, also overcoming biasing in the result. The advantages were particularly substantial in the case of low-order approximations and noisy responses.

In an analogous way to the relaxed VF method, this paper presents the modification of the recently proposed NL-VF

Received 6 April 2024; revised 27 June 2024; accepted 20 August 2024. Date of publication 26 August 2024; date of current version 25 September 2024. Paper no. TPWRD-00558-2024. (Corresponding author: Abner Ramirez.)

Abner Ramirez is with Kestrel Power Engineering, Mississauga, ON L4Z 2T1, Canada, on leave from CINVESTAV campus Guadalajara, Guadalajara 45017, Mexico (e-mail: aramirezvazquez@entrustsol.com).

Bjørn Gustavsen is with SINTEF Energy Research, N-7465 Trondheim, Norway (e-mail: bjorn.gustavsen@sintef.no).

Color versions of one or more figures in this article are available at <https://doi.org/10.1109/TPWRD.2024.3449879>.

Digital Object Identifier 10.1109/TPWRD.2024.3449879

approach for the rational identification of systems for which input/output variables are available. The relaxed condition proposed in [8], [9] is adapted and incorporated into the least-squares (LS) problem of the NL-VF formulation, whose solution provides the new poles set as the zeros of $\sigma(s)$. The computational burden of this modification is negligible, as only one equation is added to the LS problem, and the convergence behavior is improved.

The relaxed VF is comprehensively presented in Section II. Section III describes the relaxed version of NL-VF. Sections IV to VI present its validation via three systems. The first one, corresponds to the linear system analyzed in [8]. Note that, although this system is linear, it provides full insight of the relaxed NL-VF behavior. The second one is a nonlinear system involving simultaneously a photovoltaic generator and a nonlinear reactor, as presented in [5]. The third one corresponds to a field measured noisy signal. A discussion is presented in Section VII before concluding the paper in Section VIII.

II. RELAXED VF

The objective of relaxed VF [8] is to provide an N th order rational approximation of a function $f(s)$, as given by (1), where d and e are optional variables.

$$f(s) = \sum_{k=1}^N \frac{c_k}{s - p_k} + d + se. \quad (1)$$

In its first stage, relaxed VF identifies the poles of $f(s)$ by solving (2) in the least-squares sense.

$$\sigma(s)f(s) = p(s), \quad (2)$$

where

$$\sigma(s) = \sum_{k=1}^N \frac{\tilde{c}_k}{s - q_k} + \tilde{d}, \quad (3)$$

$$p(s) = \sum_{k=1}^N \frac{c_k}{s - q_k} + d + se. \quad (4)$$

In (1)–(4), $\{q_k\}$ corresponds to a set of initial poles; $\{\tilde{c}_k\}$ is the set of residues of the scaling function $\sigma(s)$; $\{c_k\}$ denotes the set of residues of the transfer function $f(s)$ (alternatively of $p(s)$); the *relaxing parameter* \tilde{d} is a real-valued variable.

In classical VF [7], we have $\tilde{d} = 1$, resulting in a high-frequency asymptote equal to unity. It was shown in [8] that this restriction impairs the pole relocation process and, as consequence, convergence properties. Such asymptotic characteristic is removed in the relaxed version of VF by introducing the parameter \tilde{d} as a free variable. This permits a larger variation of $\sigma(s)$ in the given frequency range, thereby permitting poles to be relocated a larger distance in each iteration, leading to faster convergence and a more accurate end result [8].

To prevent that the modified $\sigma(s)$ becomes zero over the frequency range under consideration; in other words, to avoid a null solution of (3), criterion (5) is added as the last equation in the LS problem, used to solve (2), where N_s is the number of frequency samples. This criterion enforces to have a non-zero

value of $\sigma(s)$, without explicitly modifying any of the free variables. Also, (5) is weighted with (6) to account for the size of $Y(s)$, as proposed in [8], with $w(s)$ being the weighting function usually defined for the fitting of a transfer function in classical VF. The use of a weighting function w allows to control the accuracy the fitting, e.g., relative error control by inverse magnitude weighting, $w(s) = 1/|f(s)|$.

$$\text{Re} \left\{ \sum_{m=1}^{N_s} \left(\sum_{k=1}^N \frac{\tilde{c}_k}{s_m - q_k} + \tilde{d} \right) \right\} = N_s, \quad (5)$$

$$\text{weight} = \frac{\|w(s) \cdot f(s)\|_2}{N_s}. \quad (6)$$

Finally, the set of zeros of $\sigma(s)$ are calculated using (7).

$$\text{eig} \left(A - b \cdot \tilde{d}^{-1} c^T \right). \quad (7)$$

In (7), A corresponds to a diagonal matrix with the set of poles as elements; b is a column vector of ones, and c^T is a row vector including the set of residues $\{\tilde{c}_k\}$; superscript T denotes transpose. The calculated zeros are used as new poles q_k in (3) and (4), giving an iterative pole relocation procedure.

III. RELAXED NL-VF

In this section, the single-port relaxed NL-VF is described, presenting the basic relations. Its extension to the multi-port case is straightforward. For further details of VF, TD-VF, and NL-VF, the reader is referred to [1], [2], [3], [4], [5], [7].

Let us suppose that the input variable, denoted as $X(s)$, and the output variable, denoted as $Y(s)$, pertain to a dynamical system and are available in the frequency domain (or in TD, followed by NLT). Then, multiplication of (2) by $X(s)$, assuming $f(s)$ as the transfer function to be identified, gives (8) with $\sigma(s)$ given in (3). This relation is evaluated in the first stage of NL-VF to calculate the zeros of the scaling function $\sigma(s)$, which are used as new initial poles in the iterative pole relocation process.

$$\sigma(s)Y(s) = \left(\sum_{k=1}^N \frac{c_k}{s - q_k} + d + se \right) X(s). \quad (8)$$

In an analogous way to relaxed VF, criterion (5) is added as the last equation in the LS problem, used to solve (8). According to the formulation of relaxed VF, (5) is now weighted with (9) to take into account the size of $Y(s)$, with w being the weight usually defined for the fitting of a transfer function in classical VF

$$\text{weight} = \frac{\|w(s) \cdot Y(s)\|_2}{N_s}. \quad (9)$$

Finally, the set of zeros of $\sigma(s)$ are calculated using (7), as given above.

As in relaxed VF, if $\tilde{d} < 10^{-8}$, the obtained solution is discarded as the calculated zeros can be inaccurate. A new LS solution is calculated with $\tilde{d} = 10^{-8}(\tilde{d}/|\tilde{d}|)$ [8].

There are two main differences in the formulations of relaxed VF and relaxed NL-VF: a) in the latter, the scaling function multiplies the output $Y(s)$, as seen in (8), instead of the (known) transfer function $f(s)$ to be fitted, as seen in (2), and b) the weight

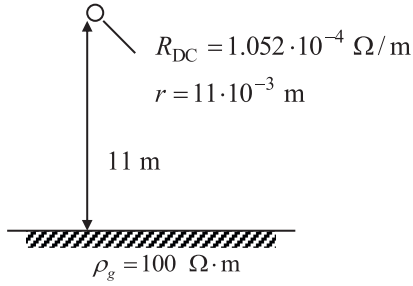
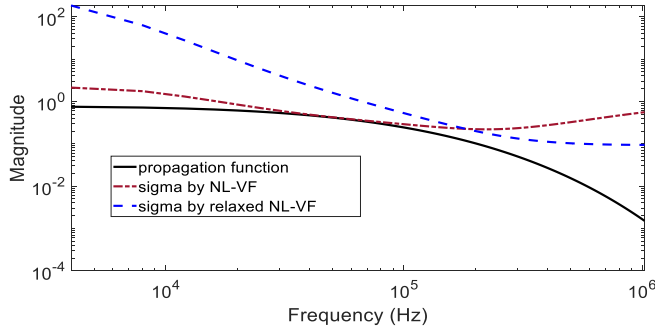


Fig. 1. Overhead line geometry.

Fig. 2. Propagation function and $\sigma(s)$ as given by NL-VF and relaxed NL-VF.

in (9) depends on $Y(s)$, instead of the (known) transfer function to be fitted. It is further emphasized that (8) applies to the case when input/output measurements of a system are available. For the case of an available transfer function, classical (or relaxed) VF can be utilized. In that case, the given transfer function $H(s)$ is an impulse response, implying $X(s) = 1$ and $Y(s) = H(s)$.

IV. EXAMPLE: SINGLE-PHASE TRANSMISSION LINE

A 25-km single-phase overhead line example, taken from [8], is presented in this section as introductory example. The line geometry is shown in Fig. 1.

The line parameters are calculated in the Laplace domain, i.e., $s = a + j\omega$, with sample values corresponding to an observation time of 0.25 ms and 512 TD samples [6]. This discretization yields $f_{max} = 1.024$ MHz and $\Delta f = 4$ kHz [6]. The input $X(s)$ is assumed to be unity, directly giving the propagation function as output $Y(s)$ [8]. Although this example corresponds to a linear component, i.e., transmission line, it provides a useful insight into the characteristics of the relaxed NL-VF approach.

For the fitting of the propagation function, seven logarithmically spaced, real poles are used. Fig. 2 presents $\sigma(s)$ as function of frequency for both NL-VF and its relaxed version. The propagation function is included, as reference, after extraction of a time delay of 83.33 μs as given by lossless line. It is observed in Fig. 2 that the variation of $\sigma(s)$, provided by NL-VF, remains close to unity along the frequency range. On the other hand, a much larger variation is exhibited by $\sigma(s)$ as given by the relaxed NL-VF, with smaller magnitudes in high frequencies. This means that $\sigma(s)$ has more zeros in high frequencies, which also means that poles are relocated toward those high frequencies

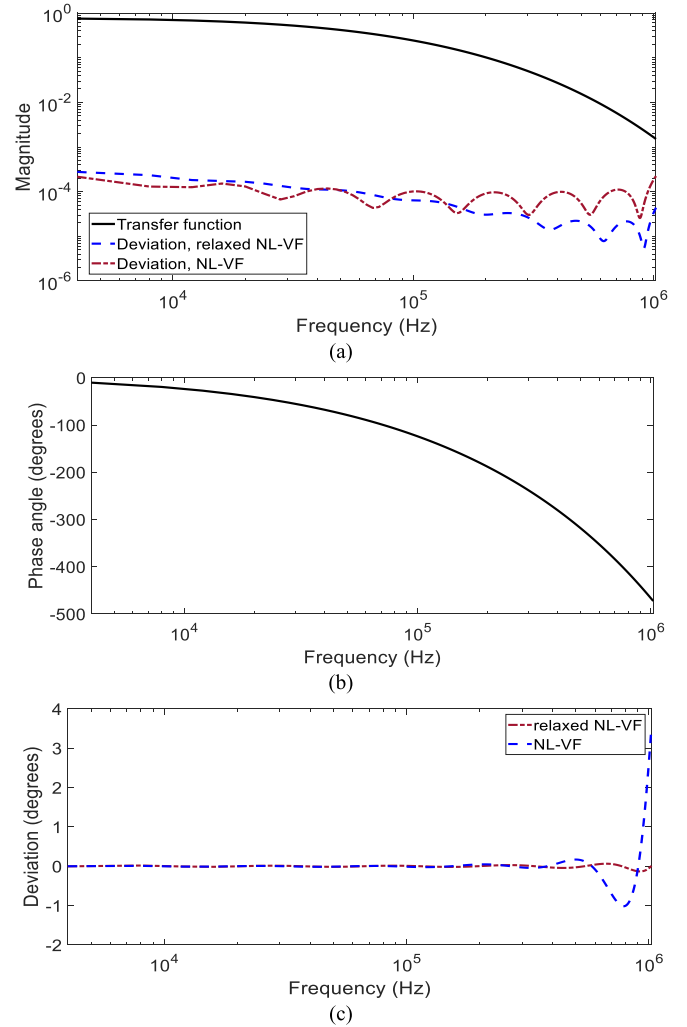


Fig. 3. Rational approximation of the propagation function as given by NL-VF and relaxed NL-VF. (a) Magnitude and deviations, (b) phase angle, and (c) phase angle deviations.

[9]. This variation confirms the better pole relocation property of the relaxed version [8], as showed in the following results. Additionally (not shown), at convergence, $\sigma(s)$ tends to unity for the complete frequency range, in agreement with the input/output relation (8) [8].

Fig. 3(a) presents the magnitude of the propagation function and the magnitude deviations, as given by NL-VF and its relaxed version, after 10 iterations. The latter provides a better approximation, especially in the high frequency range. The corresponding phase angle and deviations are presented in Fig. 3(b) and (c), respectively. It is observed that the phase angle deviation by the relaxed NL-VF is smaller than the one given by NL-VF. Fig. 4 presents the *rms* error of both methods with respect to the iteration number; the convergence characteristic of the relaxed NL-VF behaves better as compared to its original version. Also, the relaxing parameter \tilde{d} is monitored along the iterations, as shown in Fig. 5. Clearly, \tilde{d} varies substantially during the iterations.

The results in Figs. 3–5 show that the relaxed version of NL-VF provides both better fitting accuracy and convergence

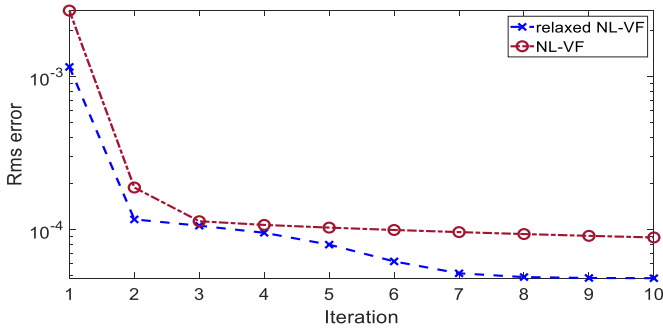


Fig. 4. Rms error by NL-VF and relaxed NL-VF as function of iteration number.

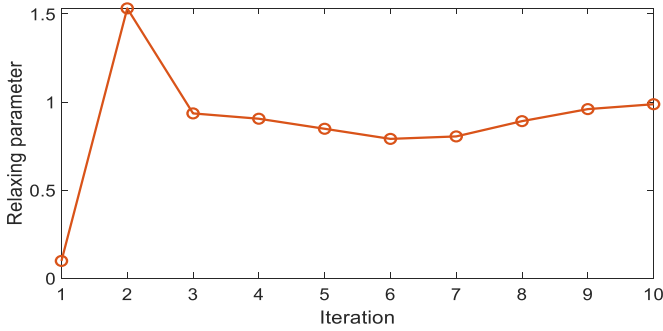


Fig. 5. Relaxing parameter as function of iteration number.

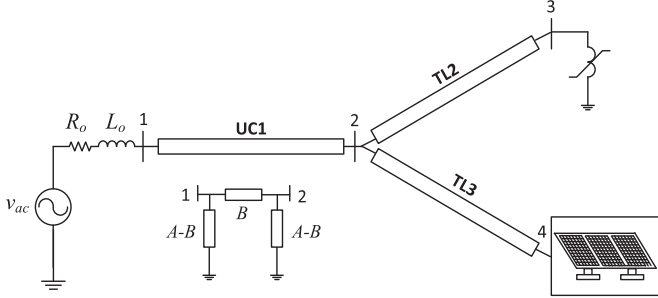


Fig. 6. Configuration of the nonlinear system used as the second example, taken from [5].

characteristics, in agreement with the conclusions in [8]. For this example, the relaxing parameter quickly reaches a unity value, as seen in Fig. 5.

V. EXAMPLE: NON-LINEAR SYSTEM

This example, taken from [5], considers a three-phase non-linear network involving one PV generator and one non-linear reactor, see Fig. 6. The underground cable (UC) and overhead transmission lines (TL) are considered as distributed parameters, frequency dependent components. The TL/UC parameters, A and B in Fig. 6, correspond to the two-port network admittances $A = Y_c \coth(\gamma l)$ and $B = Y_c \operatorname{csch}(\gamma l)$, where $Y_c = Z^{-1} \sqrt{ZY}$ is the characteristic admittance, $\gamma = \sqrt{ZY}$ corresponds to the propagation function, and l represents the TL/UC length. The reader is referred to the Appendix for the mathematical model

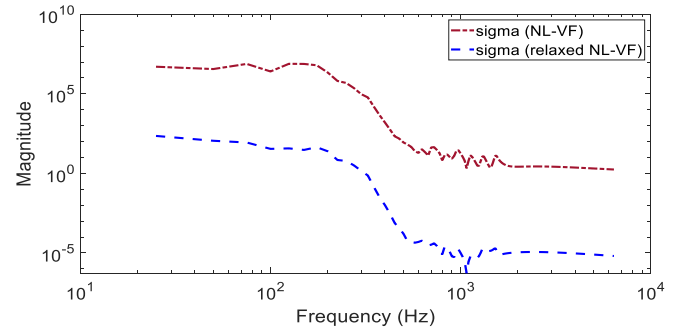


Fig. 7. $\sigma(s)$ as given by NL-VF and relaxed NL-VF.

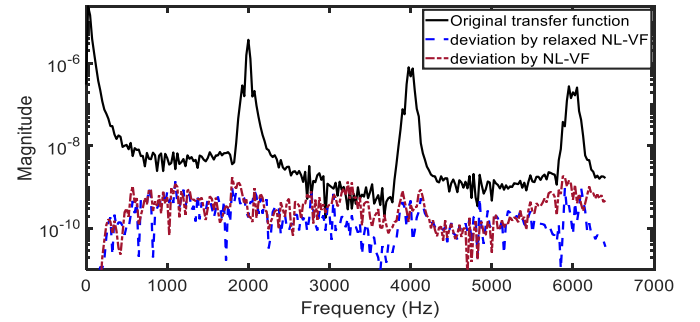


Fig. 8. Rational approximation of an arbitrary output $Y(s)$ in nonlinear system of Fig. 5, and deviations by NL-VF and relaxed NL-VF.

of the nonlinear network, including the equations for the PV generator and non-linear reactor.

The startup of the system in Fig. 6 is considered as transient scenario, considering the PV generator with specified switching parameters, i.e., no linearization is assumed [5]. The NLT is used to simulate the transient, providing frequency domain voltage/current variables amenable for the NL-VF approach. For this example, the three-phase voltage at bus 4 (v_{pcc} in Fig. 18 of the Appendix) and the three-phase current across the filter of the PV generator (i_f in Fig. 18 of the Appendix) have been chosen arbitrarily as input and output, respectively, with 512 samples each. The parameters of the PV network are listed in Table I of the Appendix.

To illustrate the improvements by the relaxed NL-VF approach, 150 initial poles are used, with 15 iterations. The initial poles are complex conjugate pairs that are logarithmically spaced along the imaginary axis.

Fig. 7 presents $\sigma(s)$, after the first iteration, given by NL-VF and its relaxed version. Note that, although similar in shape for the complete frequency range, the one by NL-VF produces values around unity for high frequencies while the one given by the relaxed version produces a very small values for high frequencies, around 10^{-5} , as seen in Fig. 7.

Fig. 8 presents the magnitude of the output's frequency domain spectrum $Y(s)$, corresponding to the arbitrarily chosen input/output pair. Also included in Fig. 8 are the deviations of the rational function approximations by NL-VF and its relaxed version.

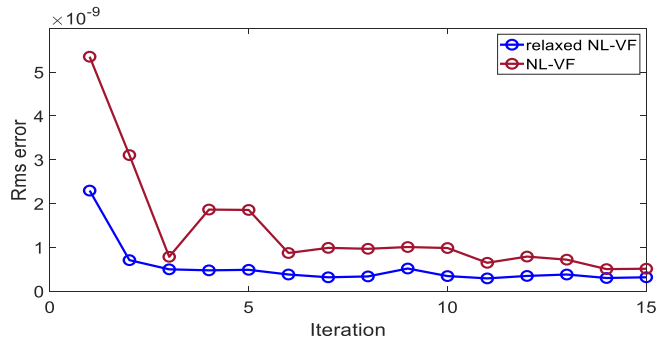


Fig. 9. RMS error by NL-VF and relaxed NL-VF as function of iteration number.

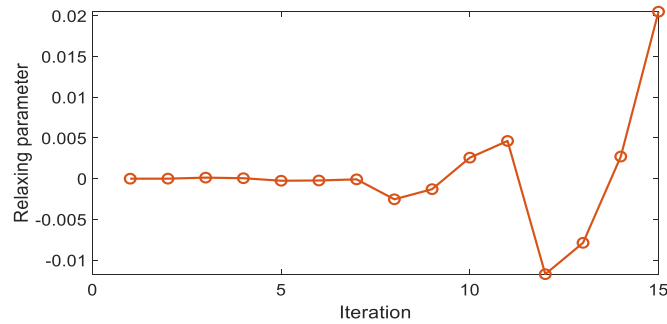


Fig. 10. Relaxing parameter as function of iteration number.

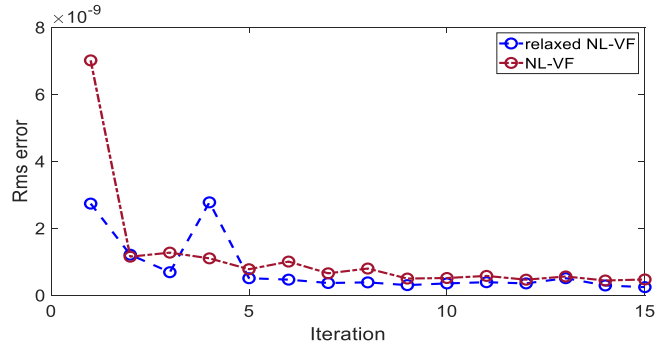


Fig. 11. RMS error by NL-VF and relaxed NL-VF as function of iteration number, considering 100 real poles.

The *rms* errors as function of the iteration number are presented in Fig. 9. As in the example of Section IV, the relaxed NL-VF yields better convergence behavior and a more accurate final result than its original version. For completeness of results, Fig. 10 shows the relaxing parameter with respect to the iteration number.

To show the ability of the proposed relaxed NL-VF to relocate poles to better positions when using a low number of poles, the initial poles now are reduced from 150 logarithmically spaced complex poles, to 100 linearly spaced real poles. Figs. 11 and 12 present the corresponding results. It is observed from these results that the relaxed NL-VF still provides better accuracy than NL-VF, despite the low number and poorly chosen placement of the initial poles.

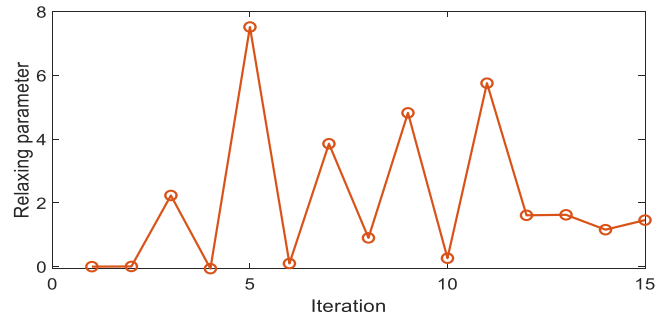


Fig. 12. Relaxing parameter as function of iteration number, considering 100 real poles.

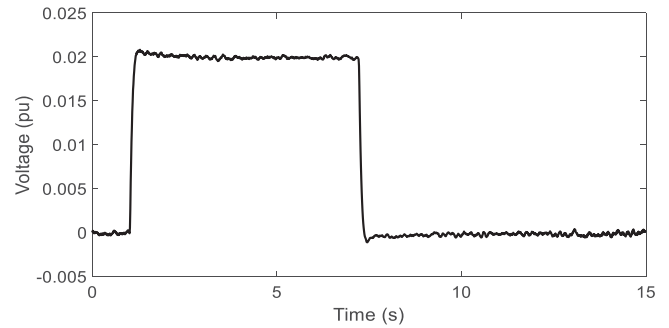


Fig. 13. Terminal voltage of a synchronous machine with an AVR system, due to a step change of a test signal. Reproduced with permission of Kestrel Power Engineering [10].

VI. EXAMPLE: MEASUREMENTS

As a final example, the automatic voltage regulator (AVR) response of a synchronous generator due to a 2% step change in a test signal is presented. This test signal is considered as input. This experimental test corresponds to classical verification of an excitation system model via online automatic voltage regulator (AVR) step response test, as per IEEE Standard 421.5 [10]. The measured terminal voltage, with 1428 samples, considered as output, is presented in Fig. 13 with permission of Kestrel Power Engineering [11]. Further details are not given due to confidentiality issues. It is observed that the measured signal is highly noisy.

For this example, 10 and 100 real poles, logarithmically spaced, are arbitrarily defined as initial pole sets. Fig. 14 shows $\sigma(s)$, as given by NL-VF and by its relaxed version. Note that with both approximation orders, the scaling function by the latter method presents smaller magnitudes at high frequencies than the one given by NL-VF which is closer to unity. As mentioned before, this characteristic of relaxed NL-VF permits a better pole relocation behavior towards high frequencies by permitting poles to be shifted a longer distance in each iteration. The improved pole relocation properties are particularly observable for the case of a poorly fitted spectrum, i.e., when using much too few poles. Such case (10 poles) is shown in Fig. 14 by the continuous blue and red traces, respectively.

Fig. 15 shows the measurement in frequency domain, and the rational function approximation by relaxed NL-VF with

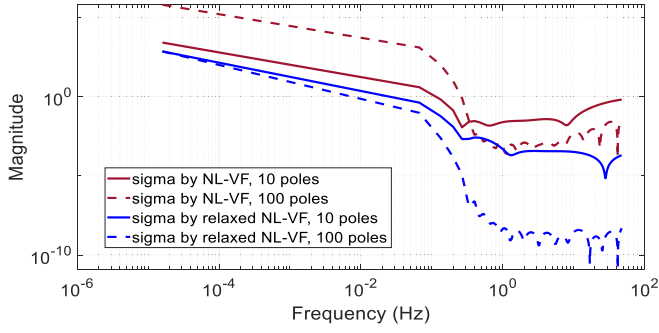


Fig. 14. $\sigma(s)$ as given by NL-VF and relaxed NL-VF.

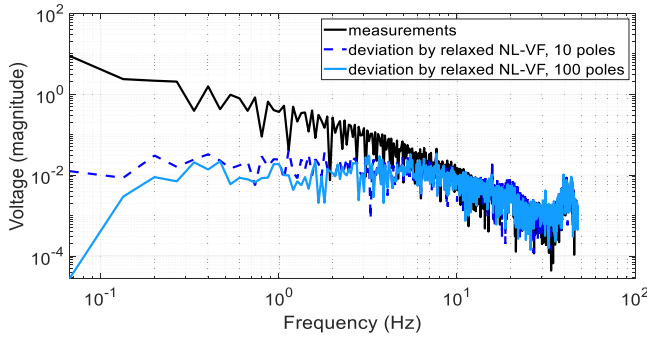


Fig. 15. Rational approximation of AVR response by relaxed NL-VF.

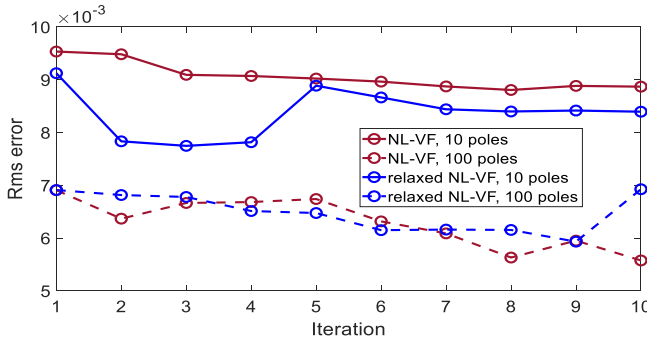


Fig. 16. RMS error by NL-VF and relaxed NL-VF as function of iteration number, considering 10 real poles.

both 10 and 100 poles. Similar results are obtained by NL-VF, but not included in Fig. 15 for clarity of presentation. The *rms* errors as function of the iteration number are presented in Fig. 16. It is observed in Fig. 16 that the relaxed NL-VF yields better convergence behavior than its original version when a low approximation order is utilized; when enough poles are used, both present in this example a similar convergence behavior.

Finally, the time domain responses of the approximation by relaxed NL-VF, with 10 and 100 poles, are compared to the measurements in Fig. 17, showing good reproduction of the wavelshape. Similar results were obtained with use of NL-VF (not shown).

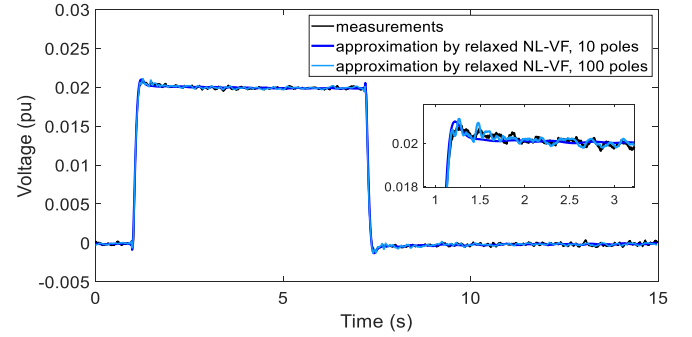


Fig. 17. Time domain waveform comparison between measurements and approximation by relaxed NL-VF.

VII. DISCUSSION

Both relaxed TD-VF and relaxed NL-VF rely on input/output signals to provide a rational approximation of a dynamical system. The system can be a linearized version of its non-linear counterpart. Then, TD-VF or NL-VF provide an identified system, valid at the assumed operating point for the linearization. Also, the input/output signals can come from a non-linear system operating at some specified conditions; for example, the PV generator in Section V involves switching functions for a given duty cycle and for given phase and amplitude of the modulating waveform. If any of those parameters change, then, and due to the non-linear characteristics of the PV system, a new identification should be computed with the new input/output signals. TD-VF and NL-VF can also identify a system whose input/output signals are obtained via measurements at its terminals, regardless of what it is inside, i.e., a black-box system. These features make TD-VF and NL-VF applicable to more general cases, as compared to classical rational approximation techniques tailored for linear systems only. As mentioned before, relaxed NL-VF is preferred due to its advantages over its counterpart TD-VF.

For further clarity, it is noted again that the word *non-linear* in NL-VF refers to the system to be identified and not to the method itself.

VIII. DISCUSSION

This paper has presented a relaxed version of NL-VF, by introducing a modified constraint in the least squares part that relates to the scaling function $\sigma(s)$, which is responsible for pole relocation. The modification, which is at no additional computational cost, permits the scaling function to attain a stronger dynamic variation, thereby allowing the poles to be shifted longer distances in each pole relocating iteration. Application to three representative examples demonstrates improvements in iteration speed and accuracy of the final result.

This relaxed NL-VF allows to calculate rational function approximations (linear models) of components and subsystems, with input data being the system input/output variables. Unlike traditional relaxed VF, which is applicable to transfer function data, the proposed method is more general. It is applicable to systems characterized by input/output responses, being either time domain data (that are converted to frequency domain using

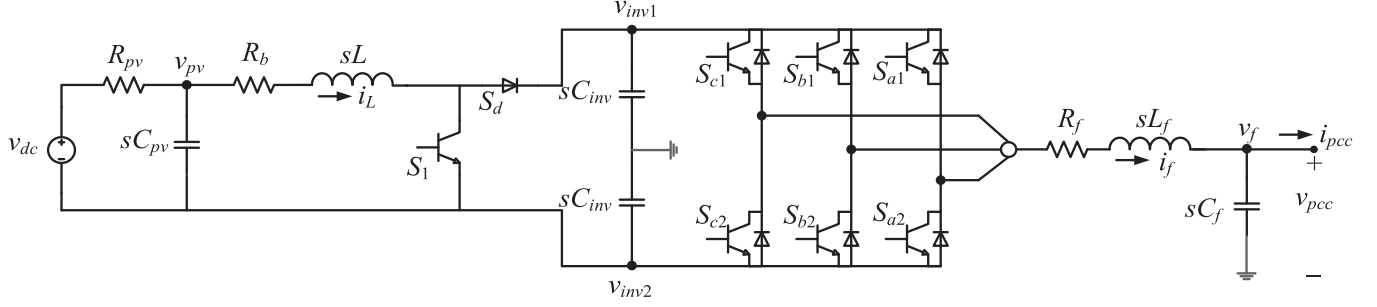


Fig. 18. Equivalent circuit for the PV generator.

NLT), or frequency domain data representing non-linear systems.

APPENDIX

The mathematical model for the three-phase PV generator of Fig. 18 is described in the following, for further details refer to [12]. Based on the variable definitions and reference directions in Fig. 18, the set of voltage/current relations in the frequency domain is given by (10).

$$v_{dc} = R_{pv}i_{pv} + v_{pv}, \quad (10a)$$

$$i_{pv} = sC_{pv}v_{pv} + i_L, \quad (10b)$$

$$v_{pv} = Z_L i_L + S_d(v_{inv1} - v_{inv2}), \quad (10c)$$

$$S_d i_L = S_{x1} i_f + Y_{Cinv} v_{inv1}, \quad (10d)$$

$$-S_d i_L = S_{x2} i_f + Y_{Cinv} v_{inv2}, \quad (10e)$$

$$S_{y1} v_{inv1} + S_{y2} v_{inv2} = Z_f i_f + v_{pcc}, \quad (10f)$$

where S_d represents a Toeplitz-type matrix corresponding to the switching function of the boost converter. The rest of variables are defined below.

Relation (11a) is obtained by performing algebraic manipulations involving (10a) to (10f).

$$Y_{eq} v_{dc} + Z_{eq} i_f = v_{pcc}. \quad (11a)$$

At the point of common coupling (PCC) between the PV generator and the rest of the network, see Fig. 18, we have:

$$i_f = Y_{Cf} v_{pcc} + i_{pcc}. \quad (11b)$$

with Z_{eq} and Y_{eq} given by (14) where S_{x1} , S_{x2} , S_{y1} , and S_{y2} involve the frequency content of the corresponding periodic time-varying TD switching functions. The combination of (11a) and (11b) gives the PV Norton equivalent, given by (12), at the PCC.

$$i_{Npv} = Y_{Npv} v_{pcc} + i_{pcc}, \quad (12)$$

where:

$$i_{Npv} = -(Z_{eq})^{-1} Y_{eq} v_{dc}, \quad (13a)$$

$$Y_{Npv} = Y_{Cf} - (Z_{eq})^{-1}. \quad (13b)$$

$$Y_{eq} = Z_d (Z_b)^{-1} Y_a, \quad (14a)$$

$$Z_{eq} = Z_e - Z_d (Z_b)^{-1} Z_c, \quad (14b)$$

with:

$$Z_a = Z_L + (Y_{Cpv})^{-1}, \quad (14c)$$

$$Z_b = Z_a + 2S_d (Y_{Cinv})^{-1} S_d, \quad (14d)$$

$$Z_c = S_d (Y_{Cinv})^{-1} (-S_{x1} + S_{x2}), \quad (14e)$$

$$Z_d = (S_{y1} - S_{y2}) (Y_{Cinv})^{-1} S_d, \quad (14f)$$

$$Z_e = -S_{y1} (Y_{Cinv})^{-1} S_{x1} - S_{y2} (Y_{Cinv})^{-1} S_{x2} - Z_f. \quad (14g)$$

Also,

$$Y_a = (Y_{Cpv})^{-1} / R_{pv}, \quad (14h)$$

$$Y_{Cpv} = sC_{pv} + 1/R_{pv}. \quad (14i)$$

$$Z_L = R_b + sL, \quad (14j)$$

$$Y_{Cf} = sC_f. \quad (14k)$$

$$Z_f = R_f + sL_f, \quad (14l)$$

$$Y_{Cinv} = sC_{inv}, \quad (14m)$$

and,

$$S_{x1} = [S_{a1} \ S_{b1} \ S_{c1}], S_{x2} = [S_{a2} \ S_{b2} \ S_{c2}], \quad (14n)$$

$$S_{y1} = [S_{a1} \ S_{b1} \ S_{c1}]^T, S_{y2} = [S_{a2} \ S_{b2} \ S_{c2}]^T. \quad (14o)$$

The nonlinear reactor model follows the relations in (15) for each phase, where φ represents the flux and $(\alpha, \beta, \text{ and } p)$ are constant values.

$$i_{nl} = \alpha \varphi + \beta \varphi^p, \quad (15a)$$

$$v_{nl} = d\varphi/dt. \quad (15b)$$

The data of the PV system in Fig. 6 are listed in Table I. As additional information, the voltage v_{pcc} and current i_f utilized as input/output variables for the rational approximation of the system in Fig. 6 are presented in Fig. 19, respectively.

TABLE I
DATA OF PV NETWORK

PV array at STC		
V_{oc}	365 V	Open-circuit voltage
I_{sc}	15.2 A	Short-circuit current
V_{mpp}	290.8 V	Voltage at MPP
I_{mpp}	14.2 A	Current at MPP
P_{max}	4129.4 W	Maximum power
N_s	468	Number of series connected cells
k_i	0.00502 A/°C	Temperature correction factor, current
k_v	-0.08 V/°C	Temperature correction factor, voltage
a	1.3	Ideality factor of diode
Boost converter		
L	9 mH	Inductance
C	2200 μ F	Capacitance
F_s	10 kHz	Switching frequency
d	0.5	Duty cycle
Voltage-sourced inverter		
F_s	5 kHz	Switching frequency
m_a	0.9	Modulating amplitude
Filter		
R_{fc}	1 m Ω	Resistance
L_{fc}	0.3 mH	Inductance
R_{fg}	1 m Ω	Resistance
L_{fg}	0.15 mH	Inductance
C_f	2.2 μ F	Capacitance

REFERENCES

- [1] S. Grivet-Talocia and B. Gustavsen, *Passive Macromodeling: Theory and Applications*. Hoboken, NJ, USA: Wiley, 2016.
- [2] S. Grivet-Talocia, "Package macromodeling via time-domain vector fitting," *IEEE Trans. Microw. Wireless Compon. Lett.*, vol. 13, no. 11, pp. 472–474, Nov. 2003.
- [3] S. D'Arco and B. Gustavsen, "Reduced order thermal modeling of power electronics modules via time domain vector fitting," in *Proc. 17th Workshop Signal Power Integrity*, Paris, France, May 2013, pp. 1–4.
- [4] A. Ubolli and B. Gustavsen, "Comparison of methods for rational approximation of simulated time-domain responses: ARMA, ZD-VF, and TD-VF," *IEEE Trans. Power Del.*, vol. 26, no. 1, pp. 279–288, Jan. 2011.
- [5] A. Ramirez, B. Gustavsen, and I. Ramirez, "Rational approximation of nonlinear systems via NL-VF," *IEEE Trans. Power Del.*, vol. 38, no. 3, pp. 1918–1926, Jun. 2023.
- [6] P. Moreno and A. Ramirez, "Implementation of the numerical Laplace transform: A review, task force on frequency domain methods for EMT studies, working group on modeling and analysis of system transients using digital simulation, general systems subcommittee, IEEE Power Engineering Society," *IEEE Trans. Power Del.*, vol. 23, no. 4, pp. 2599–2609, Oct. 2008.
- [7] B. Gustavsen and A. Semlyen, "Rational approximation of frequency domain responses by vector fitting," *IEEE Trans. Power Del.*, vol. 14, no. 3, pp. 1052–1061, Jul. 1999.
- [8] B. Gustavsen, "Improving the pole relocating properties of vector fitting," *IEEE Trans. Power Del.*, vol. 21, no. 3, pp. 1587–1592, Jul. 2006.
- [9] B. Gustavsen, "Relaxed vector fitting algorithm for rational approximation in the frequency domain," in *Proc. 10th IEEE Workshop Signal Propag. Interconnects*, Berlin, Germany, 2006, pp. 97–100.
- [10] *IEEE Recommended Practice for Excitation System Models for Power System Stability Studies*, IEEE Standard 421.5, Aug. 2016.
- [11] Kestrel Power Engineering, part of ENTRUST Solution Group, web site: Kestrel Power Engineering | ENTRUST Solutions Group.
- [12] A. Ramirez, "Frequency domain modeling of photovoltaic systems for transient analysis," *IEEE Trans. Power Del.*, vol. 37, no. 5, pp. 3762–3770, Oct. 2022.

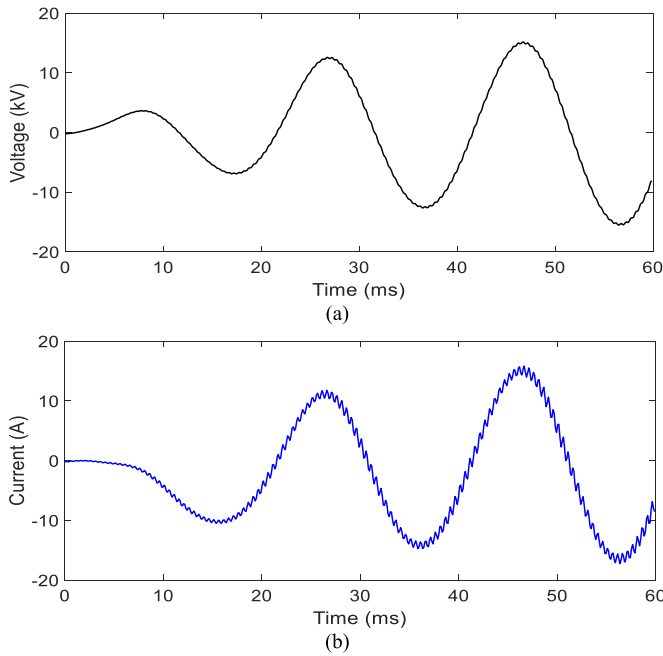


Fig. 19. Time domain waveforms corresponding to (a) voltage v_{pcc} and (b) current i_f used as input and output variables, respectively, for the rational approximation of the system in Fig. 6.

Abner Ramirez (Senior Member, IEEE) received the B.Sc. degree from the University of Guanajuato, Guanajuato, Mexico, in 1996, the M.A.Sc. degree from the University of Guadalajara, Guadalajara, Mexico, in 1998, and the Ph.D. degree from the Center for Research and Advanced Studies of Mexico (CINVESTAV), Guadalajara, in 2001. From 2001 to 2005, he was a Postdoctoral Fellow with the Department of Electrical and Computer Engineering, University of Toronto, Toronto, ON, Canada. He is currently with Kestrel Power Engineering, on leave from CINVESTAV. His research interests include electromagnetic transient analysis in power systems and power quality. He is a Member of the Mexican Association of Professionals and Entrepreneurs.

Bjørn Gustavsen (Fellow, IEEE) was born in Norway in 1965. He received the M.Sc. and Dr. Ing. degrees in electrical engineering from the Norwegian Institute of Technology (NTNU), Trondheim, Norway, in 1989 and 1993, respectively. In 1996, he was a Visiting Researcher with the University of Toronto, Toronto, ON, Canada, and with Manitoba HVDC Research Centre, Winnipeg, MB, Canada, in 1998. Since 1994, he has been with SINTEF Energy Research, where he is currently a Chief Research Scientist. Since 2020, he has also been an Adjunct Professor with NTNU. His research interests include simulation of electromagnetic transients and modeling of frequency dependent effects. He was Marie Curie Fellow with the University of Stuttgart, Stuttgart, Germany, during 2001–2002.